ARL-TR-8910 • Feb 2020

Comparison of Planar vs. Textured Silicon Carbide (SiC) Betavoltaic Devices

by Randy P Tompkins, Kasey Hogan, Claude Pullen, Iain Kierzewski, Stephen Kelley, Mohamed Doumbia, Brenda A Smith, Shadi Shahedipour-Sandvik, and Marc Litz

NOTICES

Disclaimers

ARL-TR-8910 ● Feb 2020

Comparison of Planar vs. Textured Silicon Carbide (SiC) Betavoltaic Devices

by Randy P Tompkins, Claude Pullen, and Marc Litz
Sensors and Electron Devices Directorate, CCDC Army Research Laboratory

Iain Kierzewski and Stephen Kelley
General Technical Services (GTS)

Mohamed Doumbia
College Qualified Leaders (CQL)

Kasey Hogan and Shadi Shahedipour-Sankdvik
College of Nanoscale Science and Engineering, University at Albany

Brenda A Smith
Physical Sciences Directorate, Oak Ridge National Laboratory

REPORT DOCUMENTATION PAGE						*Form Approved* *OMB No. 0704-0188*
Public reporting burden for this collection of information is estimated to average 1 hour per response, including the time for reviewing instructions, searching existing data sources, gathering and maintaining the data needed, and completing and reviewing the collection information. Send comments regarding this burden estimate or any other aspect of this collection of information, including suggestions for reducing the burden, to Department of Defense, Washington Headquarters Services, Directorate for Information Operations and Reports (0704-0188), 1215 Jefferson Davis Highway, Suite 1204, Arlington, VA 22202-4302. Respondents should be aware that notwithstanding any other provision of law, no person shall be subject to any penalty for failing to comply with a collection of information if it does not display a currently valid OMB control number. **PLEASE DO NOT RETURN YOUR FORM TO THE ABOVE ADDRESS.**						
1. REPORT DATE *(DD-MM-YYYY)* February 2020		**2. REPORT TYPE** Technical Report				**3. DATES COVERED (From - To)** 10/1/2018 – 09/30/2019
4. TITLE AND SUBTITLE Comparison of Planar vs. Textured Silicon Carbide (SiC) Betavoltaic Devices						**5a. CONTRACT NUMBER**
						5b. GRANT NUMBER
						5c. PROGRAM ELEMENT NUMBER
6. AUTHOR(S) Randy P Tompkins, Kasey Hogan, Claude Pullen, Iain Kierzewski, Stephen Kelley, Mohamed Doumbia, Brenda A Smith, Shadi Shahedipour-Sandvik, and Marc Litz						**5d. PROJECT NUMBER**
						5e. TASK NUMBER
						5f. WORK UNIT NUMBER
7. PERFORMING ORGANIZATION NAME(S) AND ADDRESS(ES) CCDC Army Research Laboratory ATTN: FCDD-RLS-CC Adelphi, MD 20783						**8. PERFORMING ORGANIZATION REPORT NUMBER** ARL-TR-8910
9. SPONSORING/MONITORING AGENCY NAME(S) AND ADDRESS(ES)						**10. SPONSOR/MONITOR'S ACRONYM(S)**
						11. SPONSOR/MONITOR'S REPORT NUMBER(S)
12. DISTRIBUTION/AVAILABILITY STATEMENT Approved for public release; distribution is unlimited.						
13. SUPPLEMENTARY NOTES						
14. ABSTRACT This technical report describes the US Army Combat Capabilities Development Command Army Research Laboratory's FY19 research effort on silicon carbide (SiC) PIN betavoltaic devices. We compare the output power of SiC betavoltaic devices in both planar and textured geometries upon deposition of liquid $^{63}NiCl_2$ radioisotopes. Our liquid radioisotope device results suggest an 8× improvement of output power in going from a planar to a textured design. This work was done in collaboration with Oak Ridge National Laboratory and the University at Albany.						
15. SUBJECT TERMS silicon carbide, SiC, betavoltaic, nickel-63, liquid radioisotopes, p-i-n diodes						
16. SECURITY CLASSIFICATION OF:				**17. LIMITATION OF ABSTRACT**	**18. NUMBER OF PAGES**	**19a. NAME OF RESPONSIBLE PERSON** Randy P Tompkins
a. REPORT Unclassified	**b. ABSTRACT** Unclassified	**c. THIS PAGE** Unclassified		UU	27	**19b. TELEPHONE NUMBER (Include area code)** (301) 394-0015

Standard Form 298 (Rev. 8/98)
Prescribed by ANSI Std. Z39.18

Contents

List of Figures

List of Tables

1. Introduction

Betavoltaic devices are useful in powering devices that require long lifetime, small size, and functionality in extreme environments (e.g., high temperature, high pressure, darkness, hostile areas). Specific Army applications requiring such a power source include wireless communication systems, unmanned aerial vehicle–persistent surveillance, unattended sensors, CubeSat power, and distributed chip power level.[1] Such applications require power in the 1-μW to 1-mW range. Betavoltaic devices operate similar to photovoltaic devices; however, instead of incident photons providing energy, radioactive isotopes emitting much more energetic beta or alpha radiation serve as the energy source. As with photovoltaics, semiconductor devices (PN, PIN, or Schottky diodes) allow for generation and collection of electron-hole pairs for useable output power. Electron-hole pairs generated by beta particles are collected in the depletion region and within one diffusion length of the edge of the depletion region.

Due to their large electronic bandgaps and high displacement energies of individual atoms, (ultra)wide bandgap semiconductors such as silicon carbide (SiC), aluminum gallium nitride ((Al)GaN), and diamond are desirable for betavoltaic applications, with GaN- and SiC-based devices found the most in this field of study.[2] Comparing GaN to SiC, each semiconductor has its advantages and disadvantages for use in this application space. SiC is an indirect bandgap semiconductor and thus has a large minority carrier diffusion length allowing for improved collection of carriers; however, it has a lower displacement energy compared to that of GaN. GaN is a direct bandgap semiconductor, thus making efficient collection of generated electron-hole pairs challenging, but it is likely a better candidate for higher-energy beta radioisotope sources due to its higher displacement energy compared to SiC.[2]

Both GaN and SiC have the advantage of well-established dry etch fabrication techniques, allowing for texturing of devices, thus increasing the overall surface area. This increased surface area due to texturing allows the potential for conformal deposition of the beta-emitting radioisotopes, thus increasing the number of beta particles that can create electron hole pairs in and near the depletion region of the device. This method is one way of increasing the output power of a single device.

In this work, we fabricate and test Widetronix Inc. 4H-SiC PIN betavoltaic devices, comparing the output power of planar versus textured devices using liquid $^{63}NiCl_2$ radioisotopes as a beta source. We also compare our liquid radioisotope device performance to analogous devices with simulated beta sources using our in-house electron beam–induced current (EBIC) instrument. Our liquid radioisotope device results suggest an 8× improvement of output power in going from a planar to a textured design. To further understand these devices, EBIC measurements were also taken to map short circuit current as a function of beam current for a constant electron energy. These EBIC results are useful for future Oak Ridge National Laboratory (ORNL) experiments where measured short circuit current can be used to estimate the amount of active $^{63}NiCl_2$ radioactive material on the device surface. All liquid radioisotope experiments were performed in collaboration with and at ORNL.

2. Experimental

2.1 ORNL Experiments

The planar and textured SiC betavoltaic devices were fabricated by Widetronix Inc. The planar device structures consist of a N+ 4H-SiC substrate, 20-µm N-layer doped at 5×10^{14} cm^{-3}, and a 200-nm P+ layer doped at 10^{19} cm^{-3}. The planar devices were in a vertical geometry with nickel as the backside ohmic contact to the substrate. Contact to the topside P+ layer was Ti/Al (30 nm/30 nm).[3] The textured device was quasi-vertical with topside p-type contact and n-type contact. The textured pattern consisted of 5.5- × 5.5-µm square pillars with spacing 4.5 µm on either side. The total etch depth was 10 µm with a total active area of the textured device 4500 × 4500 µm. This particular design was optimized for collection from a ^{3}H source; however, ^{63}Ni requires deeper anisotropic etches for an optimized structure. These etch processes are currently under development, and the optimized ^{3}H structure was used for initial ^{63}Ni experiments.

The vertical planar device was attached to the package using a conductive silver epoxy. The topside p-type contacts were wire-bonded using gold ball wire-bonding with a Market Enterprises Inc. 1204B ball bonder. The same wire-bond scheme was used for both topside P and N contacts to the textured devices.

To encapsulate the liquid radioisotope, two different methods were used to fabricate square polymer structures. A Nanoscribe Photonic Professional GT two-photon polymerization 3-D printer using their IP-S resin was used to produce 4.3-mm × 4.3-mm × 500-µm squares. The second method used a Form 2 3-D printer with high-temperature resin as the polymer to generate a 4- × 3- × 1-mm reservoir. Each different type of bottom-up generated pattern was attached directly to the device using nonconductive EA E-20HP epoxy.

Metal wires were soldered to the package for external electrical contact, and current-voltage (IV) curves were measured using a Keithley programmable curve tracer, with cables leading inside to the restricted radioisotope hood area at ORNL.

$^{63}NiCl_2$ radioisotopes were initially mixed in a 5:1 ethanol:methanol solution and subsequently deposited on the sample using a 2- to 10-µL pipet located in the restricted hood area at ORNL. After each successive deposition, the packaged devices were baked at 50 °C on a hot plate to drive off any adsorbed moisture. At each successive step, IV curves were generated and analyzed. Figure 1 shows the final packaged devices with deposited radioisotope.

Fig. 1 Fully packaged Widetronix Inc. planar and textured SiC devices loaded with $^{63}NiCl_2$ (green)

2.2 ARL EBIC

A similar planar SiC device outlined in Section 2.1 was tested at the US Army Combat Capabilities Development Command Army Research Laboratory (ARL) using an EBIC system. The system consists of a vacuum chamber evacuated to a base pressure of approximately 10^{-6} Torr, electron beam gun, xy stage for sample mounting, and output leads connected to a Keithley 2450 SourceMeter for measuring IV curves. Initially, measurements were taken at a constant electron energy of 16 keV (approximating the average energy of a ^{63}Ni beta source) as a function of beam current ranging from 0.1 to 2.4 nA. These data were used to generate a linear plot approximating the effective mCi radioactivity as a function of short circuit current (I_{sc}). These data are useful for future liquid radioisotope experiments involving $^{63}NiCl_2$ to approximate the amount deposited by observing I_{sc}. A second data set was taken, varying the incident electron energy from 1 to 16 keV with a constant beam current of 2.4 nA.

3. Results

3.1 ORNL Liquid Radioisotope Experiments

To ensure a functioning IV test setup, devices survived shipment, as well as a control measurement, dark IV curves were measured for both the planar and textured samples. These results are shown in Fig. 2, samples 3 × 6 (planar) and SN068t (textured), respectively.

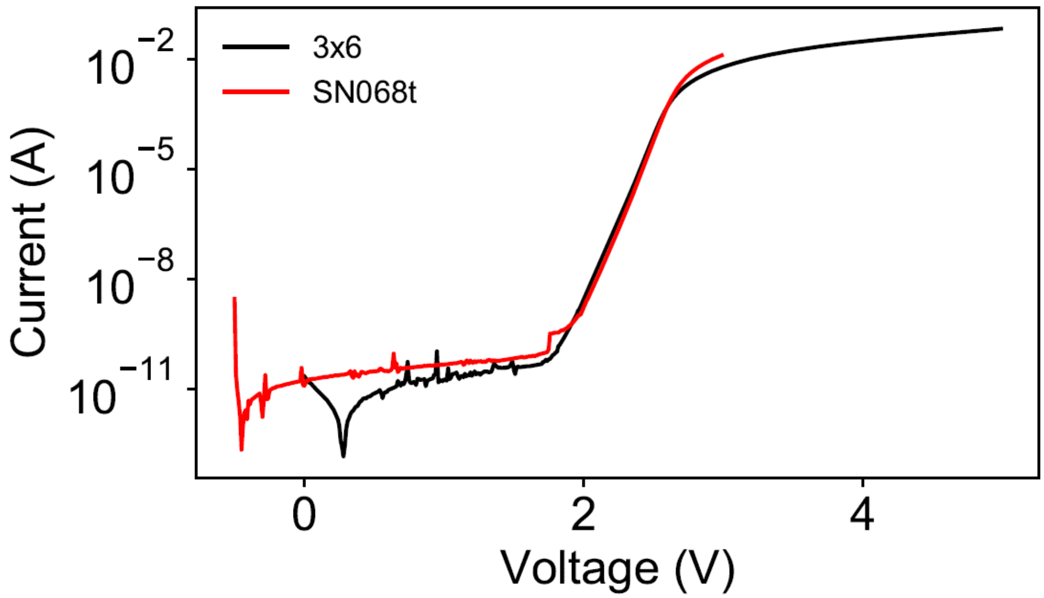

Fig. 2 Dark IV data of planar SiC device (sample 3 × 6) and textured SiC sample (SN068t). Measurement taken without exposure to ambient light.

Upon introducing the two samples into the ^{63}Ni radioisotope hood and following dark IV measurement, 100 µL of liquid $^{63}NiCl_2$ radioisotope was deposited successively onto the active area of the planar sample. IV curves were collected following each successive deposition indicated in Fig. 3. Table 1 shows analysis results from the IV curves for typical parameters of interest for betavoltaic devices, maximum power (Max P), short-circuit current (I_{sc}), open circuit voltage (V_{oc}), and fill factor (FF). The basic equations for analysis of the IV data are found in Appendix A while the Python script used to plot and analyze the data is found in Appendix B. From this analysis upon depositing 200 µL of $^{63}NiCl_2$, an output power of 1.17 µW was measured for the planar device. Numbers for both FF open circuit voltage are rather low, where V_{oc} should approximately equal the bandgap and FF for a reasonably performing device should be greater than 60%.

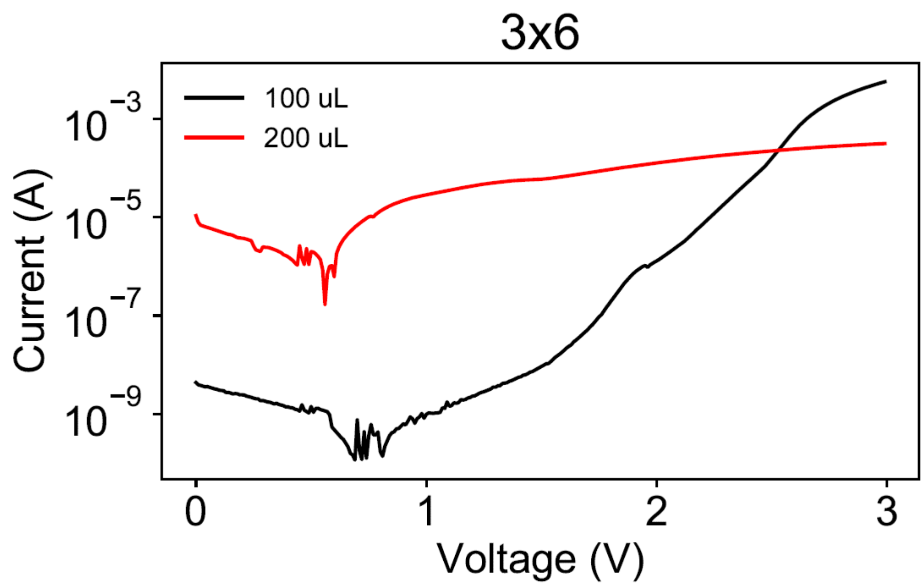

Fig. 3 **IV measurements of planar SiC sample after 100-, then 200-µL deposition of liquid radioisotope**

Table 1 **Analysis of IV curves for planar SiC betavoltaic device**

Deposited $^{63}NiCl_2$ (µL)	Max P (nW)	I_{sc} (nA)	V_{oc} (V)	FF
100	–0.708	–3.128	0.69	0.328
200	–1179.12	–5314.6	0.56	0.396

For comparison, the experiment was repeated on a textured SiC device (SN068t) with dimensions outlined in the Experimental section. This time, 50 µL of liquid $^{63}NiCl_2$ radioisotope was added in four steps for a total of 200 µL with IV curves taken immediately after each deposition to monitor the device response. IV curves generated from this experiment are shown in Fig. 4 with analysis in Table 2.

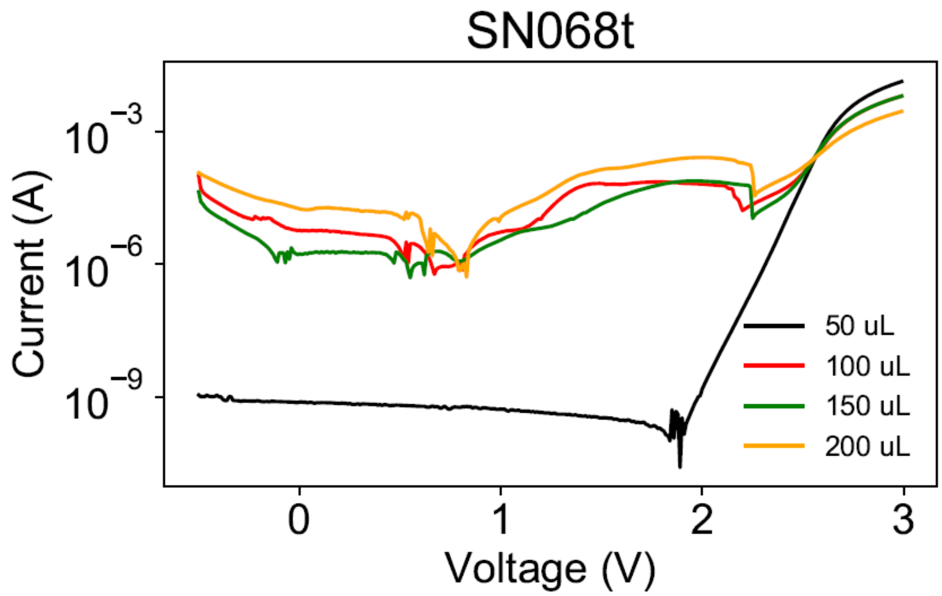

Fig. 4 IV measurements of textured SiC sample after 50-, 100-, 150-, and 200-µL deposition of liquid radioisotope

Table 2 Analysis of IV curves for textured SiC betavoltaic device

Deposited $^{63}NiCl_2$ (µL)	Max P (nW)	I_{sc} (nA)	V_{oc} (V)	FF
50	–0.9449	–0.7339	1.89	0.681
100	–1758.06	–5671.8	0.67	0.462
150	–890.03	–1833.9	0.55	0.882
200	–7901.46	–18299	0.83	0.520

Our analysis suggests a maximum output power for the textured device of about 8 µW, an 8× increase over the planar device. Interpretation of the data, specifically the changes in V_{oc} with deposition beyond 50 µL, was complicated by an increase in noise of the IV curves. However, even with difficult interpretation of V_{oc}, the data clearly show an increase in I_{sc} with increasing deposited radioisotope, indicating clear power generation. Possible reasons for this increase in noise in the data are environment (i.e., adsorption of water) or leakage of the isotope either above or beneath the reservoir shunting to the n-type contact and thus providing a short path for electron flow. Possible solutions to this problem are outlined in the Conclusions/Future Work section.

3.2 ARL EBIC Experiments

To further gauge performance of SiC PIN diodes under beta irradiation, planar SiC devices were tested using EBIC measurements as outlined in Section 2.2. The IV results of this experiment are shown in Fig. 5. The data show the expected trend of increased output power as a function of increased beam current (with the exception of low currents 0.2 and 0.3 nA). Analyses of these IV curves are shown in Table 3. Data from Table 3 are plotted in Fig. 6. Figure 7 is a plot of measured short circuit current as a function of effective radioactivity in millicurie (mCi) as approximated by the incident beam current. A linear least squares fit to these data can be used to approximate the amount of $^{63}NiCl_2$ deposited for future ORNL experiments depositing liquid radioisotopes.

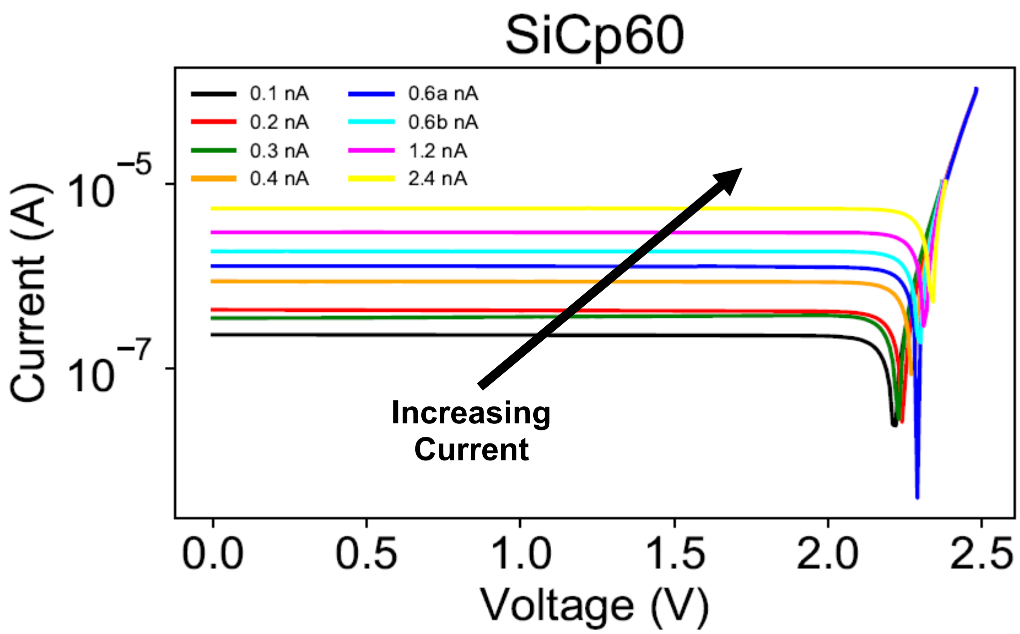

Fig. 5 EBIC measurements of a planar SiC sample with constant electron energy of 16 keV, the approximate average energy of ^{63}Ni beta source

Table 3 Analysis of EBIC results shown in Fig. 6

Beam current (nA)	Max P (µW)	I_{sc} (nA)	V_{oc} (V)	FF
0.1	–0.45	–232.5	2.22	0.874
0.2	–0.84	–431.1	2.24	0.870
0.3	–0.75	–350.9	2.23	0.969
0.4	–1.76	–874.8	2.27	0.888
0.6	–2.57	–1277.6	2.29	0.878
0.6	–3.83	–1846.1	2.30	0.901
1.2	–6.18	–2966.1	2.31	0.902
2.4	–11.27	–5351.2	2.34	0.900

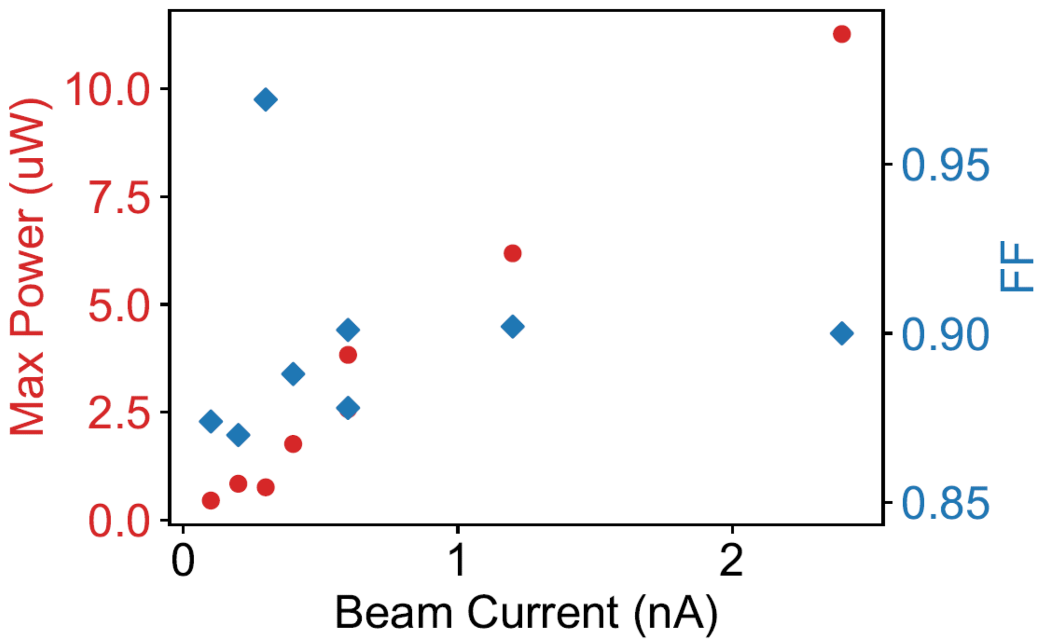

Fig. 6 Plot of maximum output power as well as FF as a function of input beam current for the planar SiC sample tested using EBIC at a constant input electron energy of 16 keV

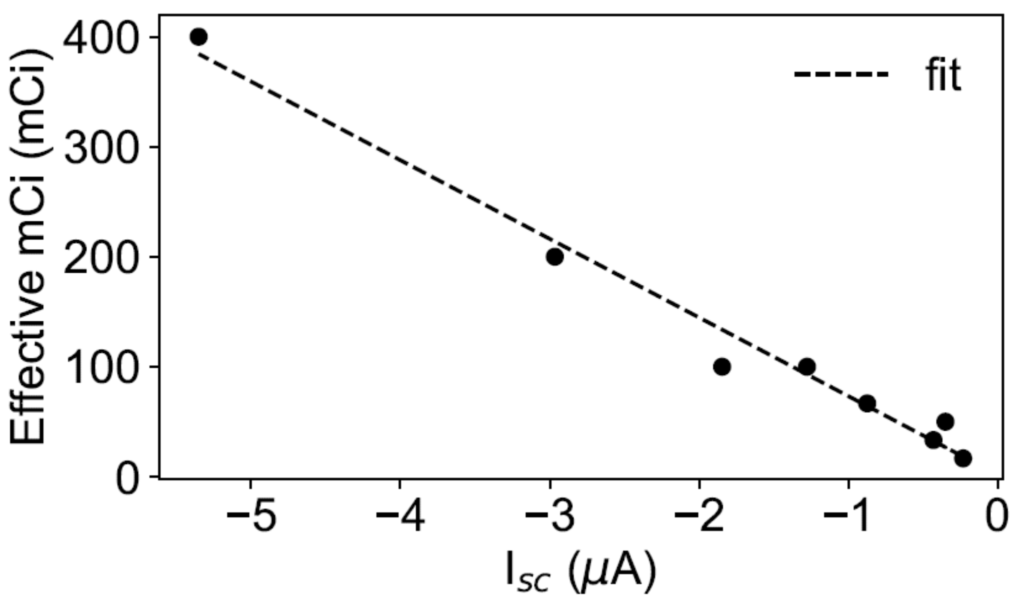

Fig. 7 Estimation of effective radioactivity as a function of short circuit current. Fit to the data: Eff_mCi = –71.5035 * I_sc + 1.6878.

The second set of EBIC experiments with the planar SiC sample included variation of the incident electron energy by changing the accelerating voltage while keeping the beam current at a constant value of 1.2 nA (estimated activity of 200 mCi based on results shown previously). The range of energies investigated (3–16 keV) encompasses the average energies of radioisotopes ^{3}H and ^{63}Ni. The IV curves generated in this experiment are shown in Fig. 8. From these IV curves the typical parameters of interest were extracted (Table 4). The efficiency is defined here as the maximum power point divided by the electron beam energy (I_{eBm} * V_{ap}). The maximum output power is plotted as a function of incident electron energy in Fig. 9. That plot of electron energy versus I_{max} does not saturate as we have seen in previous experiments for GaN.[4] This observation is due to the large electron diffusion length found in SiC compared to direct bandgap semiconductors such as GaN. Thus, a higher-energy electron gun is required to determine the saturation point.

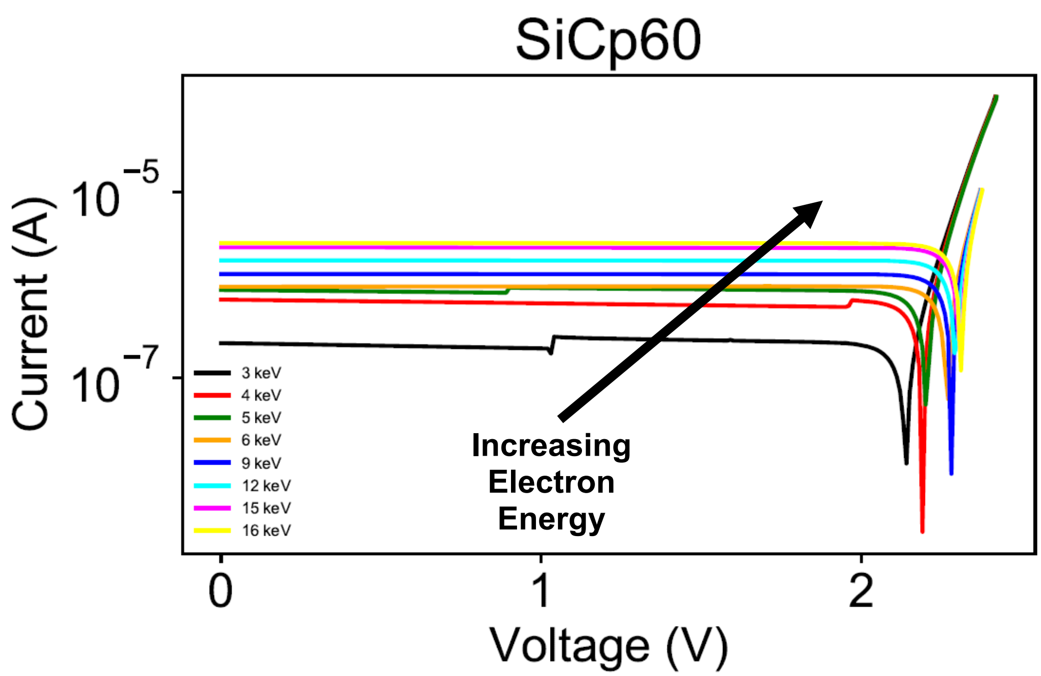

Fig. 8 EBIC measurements as a function of incident electron energy of a planar SiC sample with a constant beam current of 1.2 nA

Table 4 Analysis of EBIC results shown in Fig. 8

Electron energy (keV)	Max P (μW)	I_{sc} (nA)	V_{oc} (V)	FF	Eff
3	–0.460	–232.1	2.14	0.926	12.7%
4	–1.343	–684.4	2.19	0.896	27.9%
5	–1.702	–870.6	2.20	0.888	28.3%
6	–1.973	–949.3	2.27	0.915	27.4%
9	–2.672	–1303.3	2.28	0.899	24.7%
12	–3.784	–1826.9	2.29	0.904	26.2%
15	–5.225	–2519.8	2.31	0.897	29.0%
16	5.810	–2802.4	2.31	0.897	30.2%

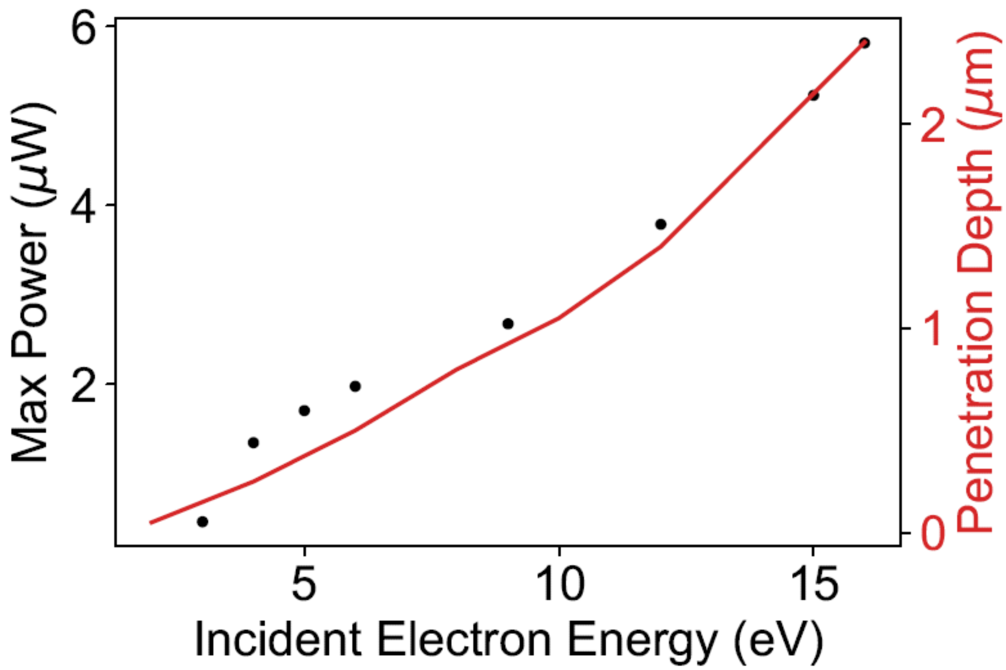

Fig. 9 EBIC results plotting both maximum output power and electron penetration depth vs. incident electron energy for the planar SiC betavoltaic device. Electron penetration depth in SiC was calculated using the continuous slowing down approximation.

Also included in Fig. 9 is the electron penetration depth versus incident electron energy as calculated using the continuously slowing down approximation (CSDA). The secondary electron yields were calculated using the two approaches. The CSDA and the energy straggler (ES) approach are very close and in agreement with the experiment. CSDA is much faster for calculation purposes because it uses as input the electron total stopping power of the material being considered. On the other hand, if other physical quantities, such as the secondary electron distributions, are required, the ES strategy should be preferred, even if it requires much longer

CPU times.[5] The ES approach results in variation in the density of secondary electron generation along the path of the incident electron.

4. Conclusions/Future Work

Liquid $^{63}NiCl_2$ beta emitter radioisotopes were deposited on both Widetronix Inc. planar and textured SiC PN diodes. Analysis of generated IV curves suggest an 8× increase in output power in going from the standard planar geometry to a textured design. EBIC measurements of equivalent planar devices suggest that the device structures are reasonably optimized as evidence by the high FF and V_{oc} > 2 V. However, independent of device design (textured vs. planar), many of the IV curves showed noise in the data as well as challenges with reproducibility of data. We attribute these results to two possible reasons: 1) environmental effects such as an uncontrolled temperature and high humidity leading to the adsorption of water and 2) possible leakage of the liquid radioisotope from the reservoirs. Adsorbed moisture to the beta source can likely attenuate beta radiation and produce changes in the IV as a function of time. Evidence of the effect of moisture on the device performance was seen in the observation that the IV curves were slightly improved with baking, but such results were short lived. Leakage of the liquid radioisotope, because the $^{63}NiCl_2$ salt has better conductivity compared to the semiconductor junction, can provide a conductive path for the electrons, thus providing a small short between the p and n contacts.

Optimization of our measurement setup is critical for future liquid radioisotope experiments. Moving forward with the goal of obtaining more reproducible data that contains less noise, these same experiments will be repeated in a controlled environment, such as a glove box with regulated humidity and temperature. Additionally, we will further seal around the perimeter of the reservoirs with an epoxy to fully contain the liquid radioisotope as well as encapsulating the wire-bond and n-type contact to prevent a conductive path if indeed leakage occurs. Placing multiple textured devices in parallel is one approach to reaching the high power levels (0.1–1 mW) needed to power Army systems. These experiments are currently underway in our FY20 efforts.

In addition to infrastructure improvements and better-sealed reservoirs, additional work in FY20 and beyond involves the use of higher-energy radioisotopes and/or texturing of more radiation hard materials such as (Al)GaN to reach output power in the range of hundreds of microwatts to 1 mW. High-energy beta sources include ^{147}Pm, ^{90}Sr, and ^{241}Am. The challenge with higher-energy radioisotopes include device degradation of the energy converter over time, which would in turn limit the net lifetime of the radioisotope battery, thus derating the power source lifetime compared to the half-life of the radioisotope of interest. The texturing approach provides challenges in both growth and fabrication, where proper growth conditions and optimized fabrication processes are required for defect mitigation as a result of either regrowth and/or dry etch processes.

5. References

1. Wacharasindhu T, Kwon J-W, Meier DE, Robertson D. Liquid-semiconductor-based micro power source using radioisotope energy conversion. Transducers 2009 – 15th International Conference on Solid-State Sensors, Actuators and Microsystems; 2009 June 21–25; Denver, CO. Piscataway (NJ): IEEE Electron Devices Society; c2009. p. 656–659.

2. Spencer MG, Alam T. High power direct energy conversion by nuclear batteries. Appl Phys Rev. 2019;6:031305.

3. Thomas C, Portnoff S, Spencer M. High efficiency 4H-SiC betavoltaic power sources using tritium radioisotopes. Appl Phys Let. 2016;108:013505.

4. Khan MR, Smith JR, Tompkins RP, Kelley S, Litz M, Russo J, Leathersich J, Shahedipour-Sandvik F, Jones KA, Iliadis A. Design and characterization of GaN p-i-n diodes for betavoltaic devices. Solid State Electron. 2017;136:24–29.

5. Dapor M. Comparison between energy straggling strategy and continuous slowing down approximation in Monte Carlo simulation of secondary electron emission of insulating materials. Prog Nucl Sci Tech. 2011;2:762–768.

Appendix A. Relevant Equations

The physics of betavoltatic devices are analogous to that of photovoltaic, with the difference being high-energy electrons as opposed to photons generating electron hole pairs. The ideal I-V characteristics of betavoltaic device is given by the equation

$$I = I_s\left(e^{\frac{qV}{kT}} - 1\right) - I_L$$

where I_s is the saturation current, q is the electron charge, V is the applied voltage, k is Boltzman's constant, T is the temperature, and I_L is the beta-generated current. The saturation current density (J_s) is given by

$$J_s = \frac{I_s}{A}$$

$$J_s = qN_C N_V\left[\frac{1}{N_A}\sqrt{\frac{D_n}{\tau_n}} + \frac{1}{N_D}\sqrt{\frac{D_p}{\tau_p}}\right]\cdot e^{\frac{-E_g}{kT}}$$

where A is the device area, N_c is the effective density of states in the conduction band, N_v is the effective density of states in the valence band, N_A is the acceptor impurity density, N_D is the donor impurity density, D_n is the electron diffusion coefficient, D_p is the hole diffusion coefficient, τ_n is the electron mean free path, τ_p is the hole mean free path, and E_g is the semiconductor electron bandgap.

A sample plot for an ideal case is shown in Fig. A-1, assuming I_L = 100 mA, I_s = 1 nA, T = 300 K, and A = 4 cm^2, typical numbers for a beta/photo voltaic device. Note that the IV curve is in quadrant IV, indicative of power generation.

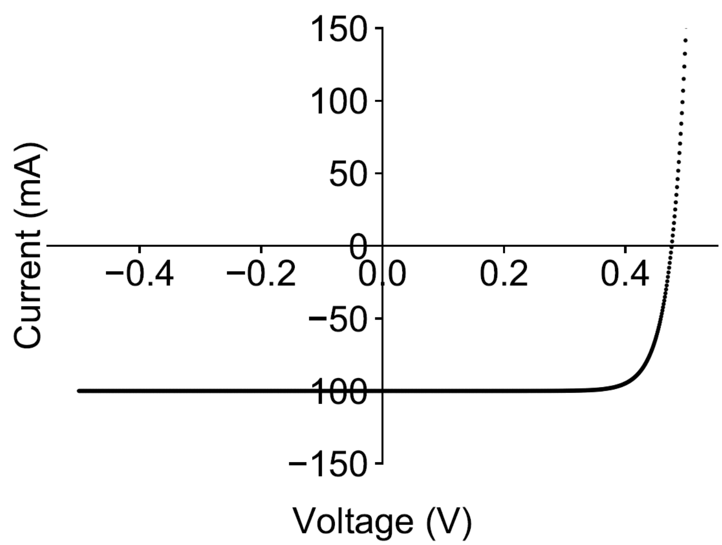

Fig. A-1 Sample IV plot of a silicon photovoltaic showing power generation

The open circuit voltage (point at which $I = 0$) is given by

$$V_{oc} = \frac{kT}{q} ln\left[\frac{I_L}{I_S} + 1\right] \cong \frac{kT}{q} ln\left[\frac{I_L}{I_S}\right]$$

Maximum power point is given by

$$P_m = I_m V_m \cong I_L\left[V_{OC} - \frac{kT}{q} ln\left[1 + \frac{qV_m}{kT}\right] - \frac{kT}{q}\right]$$

where I_m is the maximum current and V_m is the corresponding voltage at which the maximum current is measured.

The ideal power conversion efficiency is given by

$$\eta = \frac{FF \cdot I_{sc} V_{oc}}{P_m}$$

where FF is the fill factor given by

$$FF = \frac{I_m V_m}{I_{sc} V_{oc}}$$

Appendix B. Python Script

This appendix displays the Python script used to parse, plot, and analyze the IV data generated in this report.

```
# -*- coding: utf-8 -*-
# Written in Python 3
# Author: Randy Tompkins randy.tompkins.civ@mail.mil
import numpy as np
import matplotlib.pyplot as plt
from scipy import stats
import matplotlib as mpl
import os
import glob
import pandas as pd
import tkinter, tkinter.filedialog

mpl.rc('font', family='Arial', size=18)


"""
This script parses a batch of files from the Keithley 2450 Sourcemeter used for taking current-
voltage (IV) measurements of semiconductor devices. I primarily use this instrument for the
betavoltaics project, both for electron beam-induced current (EBIC) measurements as well as IV
measurements during deposition of liquid radioisotopes. The script parses the IV data, plots both
IV/PV curves and saves them as a pdf file, prints to the screen standard properties of BV devices
(FF, max power, Isc, etc.) and saves that analysis in a text file.

Because this script analyzes a batch of files, all files needing plotting/analysis should be in the
same directory as the script. All data files must be saved in a .csv format.

This is the MASTER copy of the script and should not be edited to prevent the code from
breaking.

Any questions should be directed to Dr Randy P Tompkins, randy.tompkins.civ@mail.mil,
301.394.0015.
"""

print('\n')

for filename in glob.glob("*.csv"):
    data = pd.read_csv(filename, header=7)
    data = data.to_numpy()

    voltage = data[:, 14]
    current = data[:, 1]
    power = voltage * current

    plt.yscale('log')
    plt.scatter(voltage, abs(current), s=5, marker='.', c='black')
    plt.title(filename[:-4])
    plt.xlabel('Voltage (V)')
    plt.ylabel('Current (A)')
    plt.savefig(filename[:-4]  + '.pdf' , bbox_inches='tight')
    plt.clf()

    plt.yscale('log')
    plt.scatter(voltage, voltage*abs(current), s=5, marker='.', c='black')
```

```
    plt.title(filename[:-4])
    plt.xlabel('Voltage (V)')
    plt.ylabel('Power (W)')
    plt.savefig(filename[:-4] + "_power"  + '.pdf' , bbox_inches='tight')
    plt.clf()

    # Calculate Voc, Isc, Fill Factor

    negative_current = current[current < 0]

    if negative_current.size == 0:
        print(filename + " does not contain negative values of current and thus device does not
produce power.")
    else:
        if len(negative_current) != 1:
            voltage_negative_current = voltage[:len(negative_current)]
        else:
            voltage_negative_current = voltage[0]

        open_circuit_voltage = float(voltage[int(np.where(current > 0)[0][0])])
        short_circuit_current = float(current[int(np.where(voltage > 0)[0][0])])
        max_power = min(power)
        fill_factor = float(abs(max_power) / (open_circuit_voltage * abs(short_circuit_current))) *
100

        # Print Statements
        print("RESULTS")
        print("-------")
        print("Filename: " + str(filename)[:-4] )
        print(f"V_oc = {open_circuit_voltage:.3f} V")
        print("I_sc = " + str(np.format_float_scientific(short_circuit_current, precision=2)) + " A")
        print("P_max = " + str(np.format_float_scientific(max_power, precision=2)) + " W")
        print(f"FF = {fill_factor:.2f} %")
        print("\n")

        # Results File
        results_file = open(str(filename)[:-4]  + "_RESULTS" + ".txt", "w")
        results_file.write("RESULTS" + "\n")
        results_file.write("-------\n")
        results_file.write("Filename:" + str(filename)  + "\n")
        results_file.write(f"V_oc = {open_circuit_voltage:.3f} V" + "\n")
        results_file.write("I_sc = " + str(np.format_float_scientific(short_circuit_current,
precision=2)) + " A\n")
        results_file.write("P_max = " + str(np.format_float_scientific(max_power, precision=2)) + "
W\n")
        results_file.write(f"FF = {fill_factor:.2f} %" + "\n")
        results_file.close()
```

List of Symbols, Abbreviations, and Acronyms

3-D	three-dimensional
AlGaN	aluminum gallium nitride
ARL	Army Research Laboratory
CSDA	continuously slowing down approximation
EBIC	electron beam–induced current
ES	energy straggler
FF	fill factor
FY	fiscal year
I_{sc}	short-circuit current
IV	current-voltage
Max P	maximum power
mCI	millicurie
ORNL	Oak Ridge National Laboratory
SiC	silicon carbide
V_{oc}	open circuit voltage

1 DEFENSE TECHNICAL
(PDF) INFORMATION CTR
DTIC OCA

1 CCDC ARL
(PDF) FCDD RLD CL
TECH LIB

6 CCDC ARL
(PDF) FCDD RLS CC
R TOMPKINS
M DOUMBIA
I KIERZEWSKI
M LITZ
FCDD RLS CE
C PULLEN
FCDD RLS ED
S KELLEY

2 UNIV ALBANY
(PDF) K HOGAN
S SHAHEDIPOUR-SANDVIK

1 ORNL
(PDF) BA SMITH